Polymerization as a Strategy to Improve Small Organic Matrices for Low Molecular Weight Compound Analytics with MALDI MS and MALDI MS Imaging

Kilian Horatz[†‡], Marco Giampà[§], Zhi Qiao[†‡], Siver Andreas Moestue[§&] and Franziska Lissel[†‡*]

[†]Institute of Macromolecular Chemistry, Leibniz Institute of Polymer Research Dresden, Hohe Str. 6, 01069 Dresden, Germany.

[‡]Technische Universität Dresden, Mommsenstr. 4, 01062 Dresden, Germany.

[§]MR Cancer Group, Department of Clinical and Molecular Medicine, Norwegian University of Science and Technology, Olav Kyrres Gate 9, 7030 Trondheim, Norway.

[&]Department of Pharmacy, Nord University, Universitetsallèen 11, 8026 Bodø, Norway.

ABSTRACT: High performance matrix systems are prerequisites for modern biochemical and medical investigations with MALDI MS and MALDI MS Imaging. The commonly used small organic matrices (SOMs) offer multiple advantages such as broad analyte scopes and high ionization efficiencies, and are widely accepted in the research community. Yet they also suffer from disadvantages such as strong background interferences in the low mass area (< 1000 m/z) and low vacuum stability, which is particularly detrimental for low molecular weight compound (LMWC) analytics with MALDI MS and MS Imaging. Here, we present polymerization as a strategy to alleviate these disadvantages. Vinyl groups were introduced to two well-known SOMs, 2,5-dihydroxybenzoic acid (DHB) and 7-methoxy-1-methyl-9*H*-pyrido[3,4-*b*]indole (harmine), and radical polymerization was performed to obtain polyethylene-based P(SOMs) carrying the corresponding SOMs as sidechains. The obtained P(SOMs) are fully vacuum stable and MALDI silent. Using the corresponding SOMs as benchmark, the P(SOMs) have competitive performances regarding analyte scopes and ionization efficiencies. Furthermore, both P(SOMs) are active in dual mode. To assess a future application in a clinical workflow, the P(SOMs) were applied on breast cancer xenografts and MALDI MS Imaging measurements were carried out. The P(SOMs) have the ability to produce and spatially resolve both positive and negative tissue-related ions directly from the cancer tissue. The results show that the polymerization of SOMs is a promising strategy to alleviate their disadvantages while retaining their advantages.

INTRODUCTION

"Matrix assisted laser desorption ionization mass spectrometry" (MALDI MS) and the corresponding visualization technique MALDI MS Imaging are important analytical tools in different fields, e.g. for biochemical and medical research.[1-4] In contrast to similar MS techniques, for instance secondary ion mass spectrometry (SIMS) or electrospray ionization (ESI), the analytes are incorporated in a protecting matrix, which allows to ionize them softly, preventing fragmentation or degradation. Commonly used matrix systems are small organic matrices (SOMs), which fulfill the required prerequisites of MALDI matrices, namely strong absorption of laser radiation, high crystallinity, and acidic/basic functional groups. Additional advantages are their broad analyte scope and excellent ionization efficiencies, leading to a wide acceptance in the research community. SOMs can produce matrix related signals, such as molecule ions, clusters, and fragments, preventing noise-free ("MALDI silent") measurements below 1000 m/z. This can be detrimental for certain measurements, especially when analyzing low molecular weight compounds (LMWC) with MALDI MS and MS Imaging, e.g. for drug assays and development or for disease research.[5-8] Also, SOMs often exhibit low stability in ultra-high vacuum (UHV) (~10^{-7} mbar) due to their low molar mass, which can result in an inhomogeneous matrix layer during long-term MALDI MS Imaging measurements.[9] Consequently, developing strategies to improve SOMs by alleviating their disadvantages while retaining their advantages would be interesting.

Classic SOMs for MALDI MS are organic molecules with a molar mass of <500 Da, which contain aromatic (hetero-)cycles. The conjugated π-electron system allows sufficient absorption in the UV region, the heterocyclic structure or other acidic/basic functional groups increase the ionization efficiency by (de-)protonating the analytes, and a highly crystalline morphologies ensure an efficient analyte incorporation. A good example is 2,5-dihydroxybenzoic acid (DHB), which is an excellent MALDI matrix and intensively studied regarding its analyte scope, ionization efficiency, cluster formation and MALDI sample preparation properties.[10-15] As it contains an acidic functional group, DHB is predominantly used for positive mode measurements but rare cases of negative mode measurements are also reported, yielding lower signal intensities compared to positive mode.[16-17] Due to the wide range of measurable analytes and its enhanced matrix performance, DHB is a ubiquitously used standard matrix for modern tissue analytics with MALDI MS Imaging and is frequently employed as benchmark during the development of novel or improved matrix systems.[2, 18-19] Nevertheless, DHB produces a number of matrix related signals below 1000 m/z (e.g. molecule ions, fragments, clusters) and tends to sublimate in UHV. Several strategies were

tested to counteract these disadvantages and enhance DHB's efficacy for LMWC analytics with MALDI MS and MS Imaging. Adding co-matrix systems or covalently incorporating DHB in a sol-gel silicon-dioxide polymer allowed to decrease the background interferences.[20-23] Regarding the UHV stability of DHB, it was reported that the sublimation rate of DHB is highest in the first hour under UHV, and that the sublimation rate can be decreased by converting DHB into an ionic liquid.[9, 24-25]

7-Methoxy-1-methyl-9*H*-pyrido[3,4-*b*]indole (harmine) is an effective matrix used for MALDI analytics of (sulfated-)oligosaccharides, proteins and carbohydrates.[26-30] While it is predominantly used for negative mode, harmine can also support positive mode measurements, as the presence of an acidic (secondary amine) and a basic functional group (aromatic amine) allow the ionization of the analyte in gas-phase by protonation as well as deprotonation.[29] This ability for dual mode measurements is rare for SOMs, and especially when only low amounts of analytes are available, it can be advantageous compared to mono mode matrices like DHB. The ionization efficiency of harmine as negative mode MALDI matrix is increased when ammonium chloride is added, which is advantageous for, e.g. the efficient screening of carbohydrates.[28, 30] Nevertheless, harmine produces many matrix related signals in the low mass area, such as molecule ions and clusters, and it tends to sublimate in UHV.

Next to efforts to improve established SOMs, there are also reports focused on developing novel SOMs with enhanced MALDI matrix performances, e.g. to enable a specific analyte scope, dual mode suitability, increased ionization efficiencies or low background interferences in the low mass area.[19, 31] A specific analyte scope was achieved by employing reactive functional groups such as amine-groups, which react only with compounds carrying aldehyde groups.[32] Dual mode suitability was realized by developing structures containing acidic and basic functional groups, to ionize the analytes either by protonation or deprotonation.[33-34] Also inorganic materials were shown to be efficient MALDI matrices, such as graphene (-oxide), nano particles and metal oxides.[35-37] We recently reported that conjugated polymers are promising matrices for LMWC-analytics with MALDI MS and MS Imaging as they combine very low background interferences with high vacuum stability and good ionization efficiencies in positive and negative mode.[38] Furthermore, different from classic SOMs, for conjugated polymers the analyte incorporation seems to take place in the amorphous phase.[39]

Here, we present polymerization as a new strategy to improve established SOMs. Adding vinyl groups to two well-known SOMs, DHB and harmine, followed by free radical polymerization, resulted in two novel polymeric small organic matrices (P(SOMs)) with the respective SOMs as sidechains: poly(vinyl dihydroxybenzoic acid) (**P(VDHB)**) and poly(vinyl harmine) (**P(VHar)**). Their optical properties, vacuum stabilities, and performances as MALDI matrices were tested and compared with the corresponding SOMs. Finally, the P(SOMs) were used to acquire MALDI MS Imaging heatmaps of biologically relevant samples, such as patient-derived breast cancer model xenograft, to evaluate its utility for application in preclinical studies. The results suggest that the P(SOMs) reveal similar or enhanced matrix performances compared to their corresponding SOMs, confirming polymerization as promising strategy for improving SOMs.

EXPERIMENTAL SECTION

All precursors, reagents and solvents were purchased from commercial suppliers and used without further purification. Detailed information about syntheses and experiments is given in the SI. The synthesized compounds were characterized by ^{1}H-NMR (500.13 MHz) (polymers and precursors) and ^{13}C-NMR (125.03 MHz) (only precursors) in DMSO-d_6 (Figures S2-S22). Fourier-transform-infrared-spectroscopy (FTIR) was carried out to confirm the polymerizations and post-polymerization modification (Figures S34-S41). Number average and mass average molecular weight as well as dispersity (M_n, M_w, PDI) were investigated with gel permeation chromatography (GPC) in dimethylacetamide (DMAc) and MALDI MS using *trans*-2-[3-(4-*tert*-butylphenyl)-2-methyl-2-propenylidene]malononitrile (DCTB) as secondary matrix (Figures S42-S49 and S50-S52). Additionally, the MALDI MS measurements were used to analyze the degree of polymerization (DP), the molar mass of the repeating unit and the end groups of the polymers. UV/Vis measurements were carried out in solid state (relative absorbance) and in solution (mass attenuation coefficient) for both SOMs and P(SOMs) (Figures S23-S29). The vacuum stability of the SOMs and P(SOMs) was tested by gravimetrical analysis under UHV conditions (~10^{-7} mbar) for 24h and 72h (Figures S30-S33).

All MALDI MS measurements were performed on a Bruker Autoflex Speed MALDI TOF/TOF equipped with a Smartbeam II/Nd:YAG-laser (λ = 355 nm). The "layered" dried-droplet method (V_{drop} = 1 µl) was used as sample preparation method, the matrix-to-analyte ratios are depicted in the individual mass spectra. For single analyte measurements, the commercially available lipids myristic acid (MA, M = 228 Da), linoleic acid (LA, M = 280 Da), docosahexaenoic acid (DA, M = 328 Da), dipalmitoyl-glycerol (DG, M = 569 Da), dipalmitoyl-glycerophosphocholine (DGPC, M = 734 Da) and the saccharides fructose (FT, M = 180 Da), glucuronic acid (GA, M = 194 Da), sucrose (SR, M = 342 Da), maltotriose (MT, M = 504 Da) and α-cyclodextrin (α-CD, M = 972 Da) were used. All analytes were measured in positive as well as negative reflectron mode to compare the dual mode suitability of SOMs and P(SOMs). Limit of detection (LoD) measurements of choline chloride (CC), phosphocholine (PC) and glycerophosphorylcholine (GlPC) were carried out in both polarity modes to compare the ionization efficiencies of SOMs and P(SOMs) (three individual measurements per polarity mode and per sample). Detailed information about their molar mass, molecular structures and proposed fragments are given in the SI (Table S1 and S2). The resulting spectra were plotted in six-stacked graphs for a direct comparison between SOMs and P(SOMs) with, from top to bottom: a) MS spectrum of pure sample plate, b) MS spectrum of pure analyte, c) MS spectrum of pure SOM, d) MS spectrum of analyte coated with SOM, e) MS spectrum of pure P(SOM) and f) MS spectrum of analyte coated with P(SOM). All spectra within a six-stacked plot were measured under exact same conditions to allow comparison.

The MAS98.06 patient-derived breast cancer xenograft models were established at the Institute of Cancer Research, Oslo University Hospital, as previously described.[40] Tumor tissue was orthotopically implanted into 6-week old female Hsd:Athymic Nude-Foxn1nu mice. The animals were kept under pathogen-free conditions and received supplementary 17-β-estradiol (4 µg/ml) in the drinking water. When the tumors reached a size of 200-300 mm^3, the mice received CB-839 (200 mg/kg) or placebo two times daily for 28 days, before tumors were harvested and snap-frozen in liquid nitrogen until further processing. All

procedures and experiments involving animals were approved by the Norwegian Animal Research Authority (FOTS ID: 7713 and 9126) and carried out according to the *European Convention for the Protection of Vertebrates Used for Scientific Purposes*. Cryo-sections of 10 µm, obtained using a cryostat (Leica CM 3050S), were mounted onto ITO-slides (MALDI MS Imaging-diagnostic) and stored in -80 ºC. Prior the matrix application, the sections were vacuum-dried for 10 minutes. Matrix solution (0.5 mg/ml of **P(VDHB)** and **P(VHar)** dissolved in MeOH/H_2O/acetone (50/30/20), and MeOH/H_2O (75/25), respectively) was applied using an M5-HTX sprayer and the following parameters: temperature = 80 ºC; number of passes = 6, flow rate = 0.075 ml/min, velocity = 1500 mm/s, track spacing = 2, pattern = CrissCross, pressure = 10 psi, gas flow rate = 3, dry time = 40 sec. All measurements were performed using a RapifleX MALDI Tissuetyper™ mass spectrometer (Bruker Daltonics, Bremen, Germany) equipped with a Smartbeam 3D laser under "Single" mode and with a raster rate of 1.25. The analyzer was operated in negative and positive reflectron mode, and the laser is fired at a repetition rate of 10000 Hz. External calibration was performed using red phosphorous. Positive mode measurements were acquired in the calibrated range from 61 m/z to 1400 m/z, whereas negative mode measurements were acquired in the range from 40 m/z to 1200 m/z. Further instrumental details are shown in Table S4. The samples were rastered at a lateral resolution of 70 x 70 µm (x,y) with a laser scan range of 66 µm per pixel. The MALDI MS Imaging heatmaps of histological sections were processed and evaluated by using SCiLS Lab, Version 2020a Pro and were normalized to total ion count (TIC). A weak denoising of the heatmaps was performed for a better visualization.

RESUTLS AND DISCUSSION

Design, Synthesis and Characterization

A polyethylene backbone was chosen because of its high stability due to chemical inertness, and simple and fast fabrication via radical polymerization. 2,5-dihydroxybenzoic acid (DHB) and 7-methoxy-1-methyl-9*H*-pyrido[3,4-*b*]indole (harmine) were chemically functionalized with vinyl groups and used as monomers to obtain the corresponding polymers.

For the synthesis of poly(vinyl dihydroxybenzoic acid) (**P(VDHB)**, Scheme 1) 1,4-dibromo-2,5-dimethoxybenzene (**DBrDMB**) was formylated with *n*-buthyllithium and dimethylformamide in diethylether to yield 4-bromo-2,5-dimethoxybenzaldehyde (**BrDMBA**). In the ^{1}H-NMR spectrum, a new signal at 10.27 ppm is assigned to the aldehyde proton, and the carbonyl carbon gives rise to a new signal at 188.15 ppm in the ^{13}C-NMR spectrum (Figures S2 and S3). The aldehyde was oxidized with potassium permanganate in acetone and water to give 4-bromo-2,5-dimethoxybenzoic acid (**BrDMB**), leading to the disappearance of the aldehyde proton, and the appearance of a new signal at 12.82 ppm ascribed to the acid proton (Figure S4). In the ^{13}C-NMR spectrum the carbonyl carbon C-7 is shifted to 166.43 ppm due to the lower core shielding caused by the addition of oxygen and increased oxidation state (Figure S5). The next step was the protection of the acidic group by esterification with sulfuric acid and methanol to give 4-bromo-2,5-dimethoxymethylbenzoate (**BrDMMB**). The success of this reaction was verified by an additional singlet at 3.79 ppm, belonging to the methyl ester group, and the vanishing of the acid proton signal in the ^{1}H-NMR spectrum (Figure S6). In the ^{13}C-NMR spectrum an additional signal at 52.06 ppm is observed, consistent with the ester formation (Figure S7). Then, **BrDMMB** was vinylated via Suzuki cross coupling reaction with vinylboronic acid pinacol ester in dioxane to give 4-vinyl-2,5-dimethoxymethylbenzoate (**VDMMB**). In the ^{1}H-NMR spectrum three additional doublet-of-doublet signals are observed at 5.41 ppm, 6.00 ppm and 6.95 ppm, ascribed to the protons of the vinyl group (see Figure S8 and S9). The ^{13}C-NMR spectrum exhibits an additional large signal at 130.36 ppm, assigned to the two carbons of the vinyl group (Figure S10).

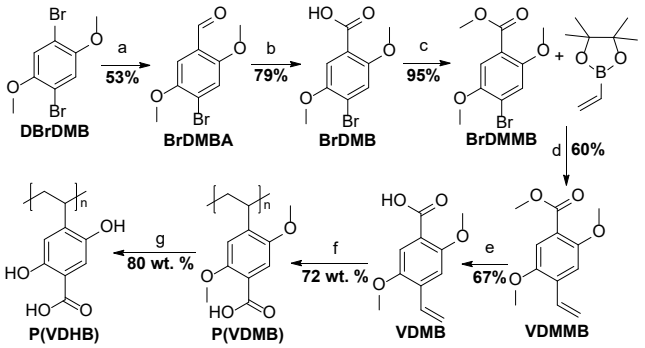

Scheme 1. Synthesis of poly(vinyl dihydroxybenzoic acid) (**P(VDHB)**). (a) *n*-BuLi, DMF, Et_2O, 1h, 0 °C-rt (b) $KMnO_4$, acetone/H_2O, 24h, rt (c) H_2SO_4, methanol, 24h, 80 °C (d) $Pd(PPh_3)_4$, Na_2CO_3, dioxane/H_2O, 72h, 100 °C (e) KOH, acetone/H_2O, 24h, 100 °C (f) AIBN, dioxane, 7h, 90 °C (g) HBr, AcOH, 5h, 120 °C.

Then, the acidic group of **VDMMB** was deprotected by hydrolysis with potassium hydroxide in acetone and water to give the monomer 4-vinyl-2,5-dimethoxybenzoic acid (**VDMB**). Its structure was verified by the vanishing of the singlet at 3.79 ppm in the ^{1}H-NMR spectrum as well as the signal at 51.85 ppm in the ^{13}C-NMR spectrum (Figures S11-S13). Afterwards, **VDMB** was polymerized to poly(vinyl dimethoxybenzoic acid) (**P(VDMB)**) via free radical polymerization using azo-bis(isobutyronitrile) (AIBN) as initiator in dioxane. The ^{1}H-NMR spectrum of **P(VDMB)** exhibits broad and partly overlapping signals. The broad signal from 9.85 - 13.67 ppm is assigned to the proton of the acidic group, whereas the signals from 4.78 - 6.71 ppm and 6.71 - 7.62 ppm are ascribed to the aromatic protons. The signal from 3.08 - 3.67 ppm belongs to the protons of the two methoxy groups and the signals from 2.22 - 2.77 ppm (including the DMSO signal) and 0.83 - 1.97 ppm originate from the protons of the ethylene-backbone (Figure S14). FTIR-spectra of both the monomer **VDMB** and the polymer **P(VDMB)** were recorded and compared (Figures S34, S35 and S39). The **VDMB** spectrum exhibits small signals in the range from 1800 - 2100 cm^{-1}, which are related to overtones of the phenyl ring. These signals vanished completely in the **P(VDMB)** spectrum due to signal broadening. Additionally, signals of C-C double bond stretching vibration at 1610 cm^{-1} and 1628 cm^{-1} in the monomer spectrum vanished and instead only one signal at 1612 cm^{-1} is observed in the polymer spectrum. Signals at 914 cm^{-1}, 968 cm^{-1} and 991 cm^{-1} in the monomer spectrum, belonging to bending vibrations of the vinyl group, completely vanished in the polymer spectrum, indicating a successful polymerization. In general, the signals in the monomer spectrum are narrower compared to the **P(VDMB)** spectrum. MALDI MS measurements of **P(VDMB)** were performed with DCTB as secondary matrix. The MALDI MS spectrum exhibits three signal series representing two dif-

ferent end group combinations, which are expected for free radical polymerization: (1) isobutyronitrile (IBN) on both sides and (2) IBN and disproportionated monomer (Figure S50 and Table S10). Both combinations are ionized by deprotonation. End group combination (2) was also detected as CN^--cluster. The averaged molar masses are $\overline{M_n}$ = 2826 g/mol and $\overline{M_w}$ = 3045 g/mol resulting in an averaged PDI of 1.08 and an averaged degree of polymerization (DP) of 15. The $\overline{PDI}$ is close to 1, so represents a narrow size distribution of the polymer chains, which is unexpected for free radical polymerizations as they usually result in broader chain length distributions (PDI ≥ 2) due to side reactions, such as recombination and disproportion.[41] An explanation for the narrow PDI could be that not all **P(VDMB)**-chains are detected with MALDI MS maybe due to too large chain lengths. The repeating unit was confirmed ($\overline{M_{RU,exp.}}$ = 208.42 ± 0.22 g/mol, $M_{RU,theo.}$ = 208.21 g/mol). GPC measurements of **P(VDMB)** were not successful, as neither a light scattering detector nor a refractive index detector could detect the sample. A possible explanation is the adsorption of the polymer on the stationary phase because of the acidic group. Finally, to obtain a polymer with free hydroxy groups, the methoxy groups of **P(VDMB)** were cleaved quantitatively post-polymerization using acetic acid and hydrobromic acid. The resulting poly(vinyl dihydroxybenzoic acid) (**P(VDHB)**) again shows broad and partly overlapping signals in the ^{1}H-NMR spectrum. The signal of the acidic proton can be observed at 12.12 - 13.61 ppm, whereas the signals of the alcohol protons are at 7.58 - 9.07 ppm and 9.43 - 11.35 ppm. The aromatic protons of the phenyl ring are at 5.08 - 6.67 ppm and 6.67 - 7.43 ppm. The protons of the ethylene-backbone are at 1.76 - 3.47 ppm (overlapping the DMSO signal) and 1.10 - 1.69 ppm (Figure S15). The integrals of the hydroxy groups cannot be used to calculate the conversion ratio because of their exchanging character. Hence, to provide an accurate conversion ratio, additionally a FTIR spectrum of **P(VDHB)** was recorded and compared with the spectrum of **P(VDMB)** (Figures S35, S36 and S40). The successful ether cleavage was verified by the complete vanishing of the signal at 1030 cm^{-1} in the **P(VDHB)** spectrum, assigned to the bending vibrations of the ether. At the same time, a signal from around 1750 - 3700 cm^{-1}in the **P(VDHB)** spectrum, which is broader and much more intense than the signal from 2300 - 3700 cm^{-1} in the **P(VDMB)** spectrum is ascribed to the hydroxy groups and indicates a high conversion ratio. Despite trying different matrices and mixing ratios, we were not able to detect the polymer **P(VDHB)** with MALDI MS. Nevertheless, the polymeric properties of **P(VDHB)** ($\overline{M_n}$, $\overline{M_w}$, $\overline{PDI}$, $\overline{DP}$) are assumed to be equal to **P(VDMB)** as the post-polymerization modification does not influence them. More detailed information including all measurement parameters are given in the SI (Table S10). Like **P(VDMB)**, **P(VDHB)** was not detected in GPC experiments, probably due to the presence of the acidic group (Figures S44 and S45). UV/Vis measurements revealed a blue-shift of the absorption maximum of **P(VDMB)** compared to **P(VDHB)** (Figure 1). This can be explained by the change of the auxochrome (methoxy to hydroxy), which influences the electron density within the phenyl ring.

Poly(vinyl harmine) (**P(VHar)**) was obtained in a facile three step reaction starting from commercially available harmine (see Scheme 2). First, harmine was brominated with *N*-bromosuccinimide in dichloromethane to obtain 8-bromo-harmine (**BrHar**). The chemical shifts and intensities of the signals observed in the ^{1}H- and ^{13}C-NMR spectra (Figures S16-S18) are consistent with literature reports.[42] Next, **BrHar** was reacted under Suzuki conditions with vinylboronic acid pinacol ester in dioxane to give 8-vinyl-harmine (**VHar**). In the ^{1}H-NMR spectrum, three additional doublet-of-doublet signals were detected at 5.58 ppm, 6.20 ppm and 7.27 ppm, originating from the three protons of the vinyl group (Figures S19 and S20). In the ^{13}C-NMR spectrum two additional signals from the vinyl group are observed at 115.93 ppm and 128.60 ppm and the signal of C-8, where the coupling is taking place, is shifted to 108.89 ppm from 92.36 ppm for **BrHar** (Figure S21).

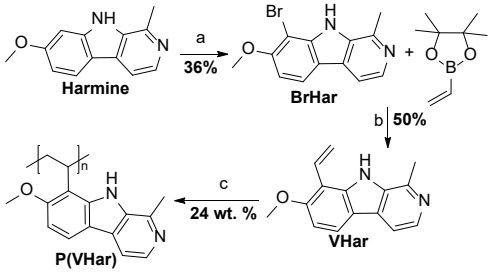

Scheme 2. Synthesis of poly(vinyl harmine) (**P(VHar)**). (a) NBS, DCM, 24h, rt (b) $Pd(PPh_3)_4$, Na_2CO_3, dioxane/H_2O, 24h, 100 °C (c) AIBN, dioxane, 7h, 90 °C.

Finally, the monomer was polymerized to the targeted polymer poly(vinyl harmine) (**P(VHar)**) via free radical polymerization in dioxane with AIBN as initiator. Consistent with a polymeric structure, the ^{1}H-NMR spectrum of **P(VHar)** reveals broad and overlapping signals (Figure S22). The signal from 5.60 - 8.71 ppm is assigned to the four aromatic protons, and the signal from 3.48 - 4.92 ppm to the three protons of the methoxy group. The signal from 1.45 - 3.15 ppm overlaps with the solvent signal of DMSO but is ascribed to the three protons of the methyl group and the proton of C-12 in the polymer backbone, which carries the sidechain. Finally, the broad signal from 0.25 - 1.37 ppm originates from the two protons of C-13, the second carbon in the polymer backbone. FTIR-spectra of the monomer **VHar** and the polymer **P(VHar)** were collected and compared (Figures S37, S38 and S41). Similar to **P(VDMB)**, the small signals in the **VHar** spectrum in the range from 1670 - 1890 cm^{-1}, which are related to overtones of the phenyl ring, vanished in the polymer spectrum, due to signal broadening. Signals at 827 cm^{-1}, 901 cm^{-1}, 928 cm^{-1} and 989 cm^{-1} in the monomer spectrum, assigned to bending vibrations of the vinyl group, vanished completely in the polymer spectrum. Signals at 1610 cm^{-1} and 1626 cm^{-1} belonging to stretching vibrations of C-C double bonds, also vanished and instead only one signal at 1618 cm^{-1} is observed in the polymer spectrum. Again, the signals in the monomer spectrum are narrower compared to the polymer spectrum. In MALDI MS measurements performed in positive reflectron mode with DCTB as secondary matrix, three different end group combinations were detected, which are expected for free radical polymerization: (1) IBN and disproportionated monomer, (2) IBN on both sides and (3) disproportionated monomer on both sides. All were ionized by protonation. The averaged molar masses are $\overline{M_n}$ = 3031 g/mol and $\overline{M_w}$ = 3610 g/mol, resulting in an averaged PDI of 1.19 and an averaged degree of polymerization (DP) of 15. This $\overline{PDI}$ is larger than the $\overline{PDI}$ of **P(VDMB)** but still represents a narrower chain length distribution than expected for a free radical polymerization (PDI ≥ 2).[41] The molar mass of the repeating unit was confirmed ($\overline{M_{RU,exp.}}$ = 238.26 ± 0.16 g/mol, $M_{RU,theo.}$ = 238.29 g/mol) (Figure S51 and Table S12). GPC measurements in dimethylacetamide (DMAc) gave different

values (Figures S46 and S48 and Table S8): $\overline{M_n}$ = 12100 g/mol, $\overline{M_w}$ = 13000 g/mol and $\overline{PDI}$ = 1.07. A possible explanation for the difference between GPC and MALDI values is that the polymer chains detected with GPC are not detected with MALDI MS. Contrary, the polymer chains detected with MALDI MS are also observed in the LS-chromatogram (GPC) as low-intensity signal at 8.59 minutes elution time (Figure S47). An extrapolation of the molar mass curve showed that the molar chain mass at 8.59 minutes elution time corresponds to the chain masses observed in the MALDI MS spectrum (Figure S49 and Table S9). Consequently, with MALDI MS only short polymer chains are detected, which are the minor part of the polymer as indicated by GPC signal intensities. In order to detect also the large polymer chains, a MALDI MS measurement in linear positive mode was carried out (Figure S52) using identical parameters as for the reflectron mode measurement. The linear mode spectrum shows three signal series in the same mass range as the reflectron mode spectrum but with less resolved signals. Longer chains of **P(VHar)** could not be detected.

Optical properties

To be suitable as MALDI matrix, a compound must absorb efficiently at the wavelength of the equipped laser (here: λ_{laser} = 355 nm). To compare the optical properties of the newly synthesized polymeric matrices with the related SOMs, first the relative absorbance of all compounds as drop-casted thin films (Figure 1, dashed lines) was recorded, as this is similar to the MALDI sample preparation conditions. Next, the mass attenuation coefficient (MAC)[43] was calculated from UV/Vis spectra collected in methanol solution to directly compare the absorption efficiencies of SOMs and P(SOMs) at the laser wavelength (Figure 1, regular lines). Detailed information about sample preparation, measurement conditions, calculations and all results is given in the SI (Figures S23-S29, Table S5, S6 and S7).

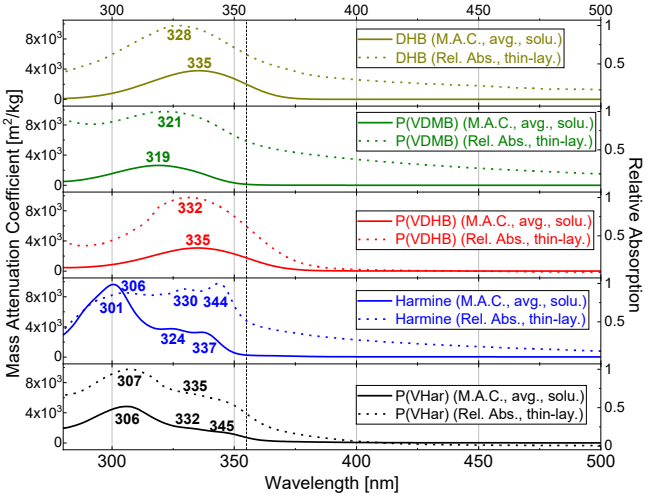

Figure 1. Optical measurements of the relative absorbance (dashed) and the averaged MAC (straight). From top to bottom: DHB (yellow), **P(VDMB)** (green), **P(VDHB)** (red), Harmine (blue) and **P(VHar)** (black).

As thin film, DHB and **P(VDHB)** reveal identical relative absorption of $A_{rel.,355}$ = 62% at the laser wavelength (355 nm), and the precursor-polymer **P(VDMB)** exhibits similar $A_{rel.,355}$ = 61%, indicating equal absorption efficiencies. Thin film samples of harmine show a higher relative absorbance ($A_{rel.,355}$ = 51%) than **P(VHar)** ($A_{rel.,355}$ = 42%), suggesting that harmine absorbs more efficiently than **P(VHar)** in solid state.

In solution, DHB and **P(VDHB)** exhibit narrow averaged MACs at the laser wavelength (DHB: $\overline{MAC_{355}}$ = 1993.6 m²/kg, **P(VDHB)**: $\overline{MAC_{355}}$ = 1760.2 m²/kg). The MAC of **P(VDHB)** is thus slightly lower (-11.7%), but still high enough to indicate good absorption efficiency. The precursor-polymer **P(VDMB)** on the other hand exhibits a much lower averaged MAC_{355} of 132.7 m²/kg (-93.3%), probably due to the different auxochrome as described above. The $\overline{MAC_{355}}$ of harmine is 265.6 m²/kg, whereas **P(VHar)** has a $\overline{MAC_{355}}$ of 729.3 m²/kg (+274.6%), indicating a higher absorption efficiency of **P(VHar)**.

Vacuum stability

MALDI MS measurements are performed under UHV (~10^{-7} mbar), which can cause SOMs to sublimate. Especially during MALDI MS Imaging measurements, which can take several hours, this can change the amount of matrix on individual measurement spots. Contrary to SOMs, polymers are vacuum stable due to their high molar mass. The vacuum stability of the SOMs and P(SOMs) was measured by keeping them as thin films under UHV and determining the weight loss after defined intervals. In Figure 2, the relative masses of the SOMs and P(SOMs) are plotted against time under UHV. For both DHB and harmine, the largest mass loss occurs within the first 30 minutes under UHV (DHB: 5.3%; harmine: 6.7%). Afterwards the mass loss rate slows down, resulting in an exponential decrease during the first 6h. For DHB, this is consistent with literature.[9] Measurements from 0h - 24h show that the exponential decrease continues for both SOMs, with DHB and harmine experiencing 16% and 14% total loss, respectively. A further measurement after 72h under UHV showed a total loss of 29% for DHB and 28% for harmine (Figure S30 and S33). As expected, these results confirm that both SOMs have a tendency to sublimate, a potential disadvantage for long term MALDI MS Imaging measurements under UHV. Also, the weight loss curves suggest that for both DHB and harmine, it might be advantageous to start MALDI MS Imaging experiments after 2h in UHV to utilize the lower sublimation rate to achieve a good spot-to-spot reproducibility.[44]

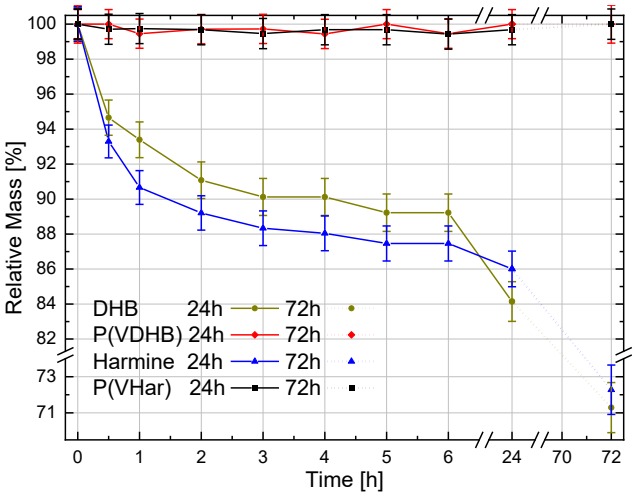

Figure 2. Vacuum stability measurements under UHV (~10^{-7} mbar) over 24h (average of 3 measurements, straight plots) and 72h (single measurements, dashed plots) of DHB (yellow), **P(VDHB)** (red), harmine (blue) and **P(VHar)** (black). The balance error of 0.01 mg is visualized relative to the sample weight as error bars.

In line with expectations, neither **P(VDHB)** nor **P(VHar)** showed significant mass changes over time under UHV conditions. Even after 24h and 72h the polymer masses were fully retained, indicating that the P(SOMs) are completely vacuum stable.

P(SOMs) as MALDI matrices

Despite potential drawbacks regarding vacuum stability and interferences in the low mass area, SOMs are excellent matrices due to their broad analyte scopes and high ionization efficiencies. Consequently, every new matrix system needs to be benchmarked against this. Polymerizing should ideally retain performances regarding scopes and efficiencies and alleviate the background interferences and vacuum instability. To verify this hypothesis, the matrix performances regarding analyte scopes, dual mode suitability, background interferences and ionization efficiencies of SOMs and P(SOMs) were compared using identical MALDI MS measurement conditions. Five commercially available lipids were used as standard DHB analytes (myristic acid (MA), linoleic acid (LA), docosahexaenoic acid (DA), dipalmitoyl-glycerol (DG) and dipalmitoyl-glycero-phosphocholine (DGPC)) and five commercially available saccharides as standard harmine analytes (fructose (FT), glucuronic acid (GA), sucrose (SR), maltotriose (MT) and α-cyclodextrin (α-CD)). All analytes were used for single analyte measurements with DHB and **P(VDHB)** as well as harmine and **P(VHar)** in both positive and negative reflectron mode. In addition, three choline derivatives (choline chloride (CC), phosphocholine (PC), glycerophosphocholine (GlPC)), which are biologically relevant metabolites for cancer research, were used for limit of detection (LoD) measurements, again in both polarity modes.[45] The molecular masses and structures of all analytes are given in the SI (Table SXX and SXX).

MALDI MS Measurements of Single Analytes - P(VDHB). All analytes measured with DHB were also detected using **P(VDHB)**, indicating comparable analyte scope (Figures S53-S71). Despite the slightly lower MAC, **P(VDHB)** required an identical or lower laser intensity than DHB for the detection of all lipids and saccharides, which indicates an enhanced ionization efficiency of **P(VDHB)** under the given conditions (Figure 3). The analyte α-CD in negative mode observed with either DHB or **P(VDHB)**, despite testing different sample preparation and measurement conditions (Table SXX). S22). Although DHB and hence also **P(VDHB)** are predominantly used for positive mode measurements, the negative mode measurements indicate dual mode suitability for both matrices. For DHB, the dual mode use was previously reported, showing that DHB produces lower intense analyte signals in negative mode than in positive mode.[16-17] In all DHB spectra, matrix related signals originating from molecule ions, fragments and clusters were detected. The **P(VDHB)** spectra reveal no matrix related signals (Figure 3), making **P(VDHB)** a MALDI silent matrix under the used measurement conditions.

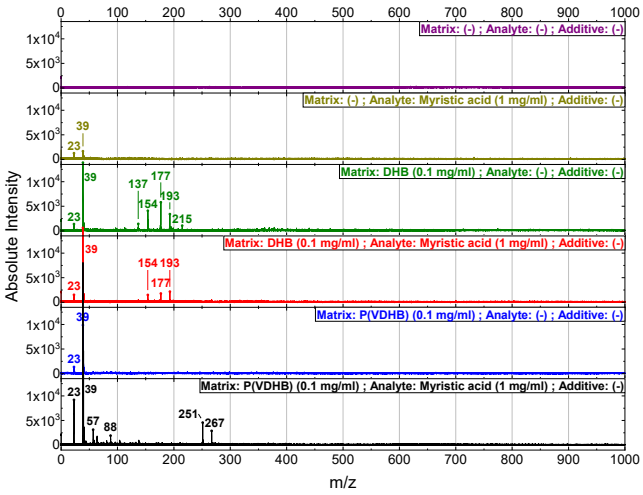

Figure 3. Reflectron positive mode (30% laser intensity) MALDI MS spectra of (a) sample plate (violet), (b) only pure analyte MA (yellow), (c) only pure DHB (green), (d) DHB coated on MA (red), (e) only pure **P(VDHB)** (blue), and (f) **P(VDHB)** coated on MA (black). Peaks: m/z = 23 $[Na]^+$; 39 $[K]^+$; 57 $[MA1=C_4H_9]^+$; 88 $[MA2=C_4H_8O_2]^+$; 137 $[DHB\text{-}OH^-]^+$; 154 $[DHB]^{\bullet+}$; 177 $[DHB+Na^+]^+$; 193 $[DHB+K^+]^+$; 215 [unknown DHB signal]$^+$;[38] 251 $[MA+Na^+]^+$; 267 $[MA+K^+]^+$.

MALDI MS Measurements of Single Analytes - P(VHar). Apart from α-CD, which was only detected with harmine, **P(VHar)** shows a similar analyte scope compared to harmine (Figure 4, Figures S72-S91). Also for the pair **P(VHar)** and harmine, the P(SOM) required an identical or lower laser intensity to detect the analytes, indicating enhanced ionization efficiency. α-CD in negative mode was only detected with harmine at high laser intensity (90%) but not detected with **P(VHar)** despite testing different conditions (Figure S81 and Table S42). Like harmine, **P(VHar)** is suitable for measurements in both positive and negative mode. In both polarity modes, harmine produces matrix related signals, i.e. molecule ions and clusters. **P(VHar)** on the other hand produces no such signals, indicating that **P(VHar)** is a MALDI silent matrix.

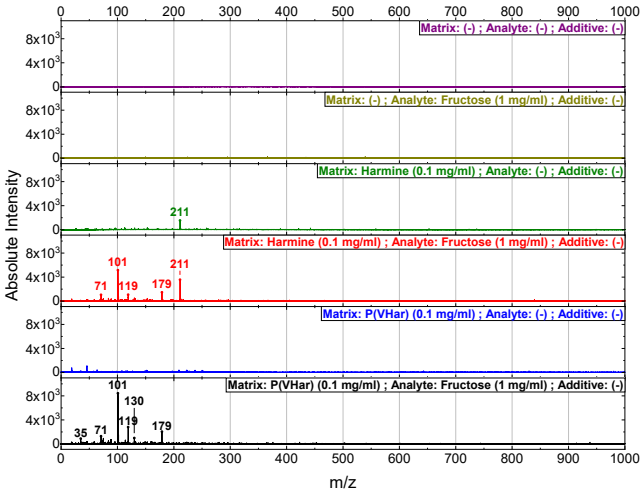

Figure 4. Reflectron negative mode (30% laser intensity) MALDI MS spectra of (a) sample plate (violet), (b) only pure analyte FT (yellow), (c) only pure harmine (green), (d) harmine coated on FT (red), (e) only pure **P(VHar)** (blue), and (f) **P(VHar)** coated on FT (black). Peaks: m/z = 35 $[Cl]^-$; 71 $[FT1=C_3H_3O_2]^-$; 101 $[FT2=C_4H_5O_3]^-$; 119 $[FT3=C_4H_7O_4]^-$; 130 $[FT4=C_6H_{10}O_3]^-$; 179 $[FT\text{-}H^+]^-$; 211 $[Har\text{-}H^+]^-$.

Limit of Detection (LoD) Measurements. To compare the ionization efficiencies of SOMs and P(SOMs) LoD measurements were carried out using different choline derivatives, which are biologically relevant metabolites in cancer research. Due to the ionic character of choline chloride (CC), it was detected only in positive mode as the cationic molecule ion of choline (M = 104 Da) and a fragment (M = 86 m/z[46]). These ions were also observed without matrix but with DHB as well as **P(VDHB)**, they were more intense and still detected at concentrations of 960 amol (Figures S94-S96). With harmine and **P(VHar)**, CC was observed down to concentrations of 9.6 pmol (Figures S97-S99). In these experiments, both P(SOMs) have the same detection limit for CC as their corresponding SOMs.

MALDI MS measurements of pure phosphocholine (PC) and glycerophosphocholine (GlPC) were carried out without matrix in both polarity modes determine the most promising analyte signals for the LoD measurements (Figures S100 and S117). High laser intensities (90%) were needed to obtain suitable signals, which were afterwards filtered according to their intensities relative to other analyte signals and their ability to uniquely represent the individual analyte. For PC, the signals at 122 m/z (positive mode) and 161 m/z (negative mode) were chosen, for GlPC the signals at 139 m/z (positive mode) and 242 m/z (negative mode). All LoD measurements were performed using 40% laser intensity. In positive mode LoD measurements of PC using DHB and **P(VDHB)**, the signal at 122 m/z was still detected at concentrations of 540 pmol, whereas in negative mode the signal at 161 m/z was observed down to concentrations of 5.4 nmol (Table 1, Figures S101-S108). Similarly, when measuring GlPC in positive mode, the signal at 139 m/z was still observed at concentrations of 390 pmol and in the negative mode the signal at 242 m/z was detected down to concentrations of 3.9 nmol, using either DHB or **P(VDHB)** (Figures S118-S125). Consistent with the CC measurements, these results indicate comparable ionization efficiencies for DHB and **P(VDHB)**.

A similar trend was observed for harmine and **P(VHar)**: While the detection in positive mode is more sensitive, SOM and P(SOM) detect PC and GlPC down to the same concentrations (see Table 1, S109-S116 and S126-S133).

Table 1. Minimal concentrations of CC, PC and GlPC detected with DHB & **P(VDHB)** and harmine & **P(VHar)**.

	DHB & P(VDHB)		**Harmine & P(VHar)**	
	Positive	Negative	Positive	Negative
CC	960 amol	n/a	9.6 pmol	n/a
PC	540 pmol	5.4 nmol	540 pmol	5.4 nmol
GlPC	390 pmol	3.9 nmol	390 pmol	3.9 nmol

MALDI MS Imaging. After verifying that the matrix performances regarding analyte scopes, ionization efficiencies and dual mode suitability of the P(SOMs) are comparable to the corresponding SOMs, their ability to detect multiple compounds directly on biologically relevant tissue sections was tested: **P(VDHB)** and **P(VHar)** were employed as matrix to analyze cryosections of tumor tissue from a breast cancer xenograft model by MALDI MS Imaging.

Fehler! Verweisquelle konnte nicht gefunden werden. shows the heatmaps of MALDI generated cations using **P(VDHB)** and the corresponding optical picture. The spatial localization of positive ions (m/z = 72.1; 229.8; 360.7; 462.6; 666.4; 794.4; 874.5 and 920.4) is tissue specific, as the ions are localized mainly in the tissue. Although the tissue section predominantly consists of neoplastic tissue, the ions display different spatial concentrations. This is consistent with the intratumoral physiological heterogeneity previously described in this xenograft model (Ref: Huuse EM et al J Magnetic Reson Imaging 2012 and Moestue S et al Breast Cancer Research 2013) Similar to single analyte measurements, sufficient heatmaps using **P(VDHB)** in negative mode were measured and depicted in Figure 6, showing the spatial distribution of negative ions localized on the tissue (m/z = 99.0, 166.9, 281.2, 324.7, 428.7, 465.6, 518.6, 764.4). Like in positive mode, the negative mode heatmaps display spatial variability in ion concentration. The experiments verify the dual mode suitability for P(VDHB) also as MALDI MS Imaging matrix. More detailed pictures of the heatmaps are depicted in the SI (Figures S137-S152).

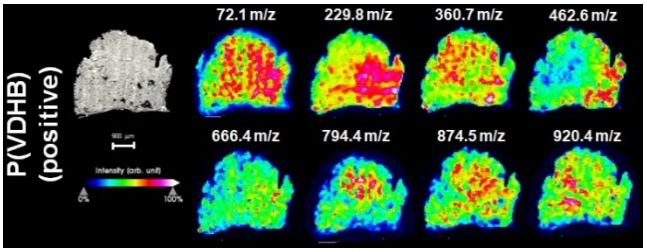

Figure 5. Positive mode MALDI MS Imaging measurements of a cryosection from a patient-derived breast cancer xenograft tumor using **P(VDHB)** as matrix. Top (from left to right): optical picture, ionic intensity heatmaps of ions at m/z values 72.1, 229.8, 360.7, 462.6. Bottom (from left to right): ionic intensity heatmaps of the ions at m/z values 666.4, 794.4, 874.5, 920.4.

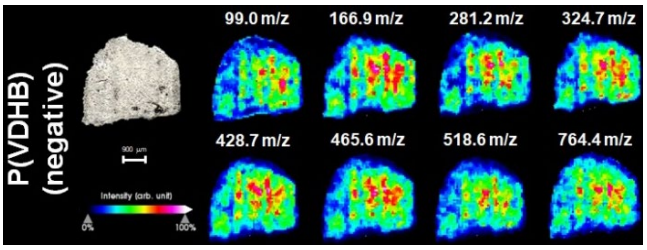

Figure 6. Negative mode MALDI MS Imaging measurements of a cryosection from a patient-derived breast cancer xenograft tumor using **P(VDHB)** as matrix. Top (from left to right): optical picture, ionic intensity heatmaps of ions at m/z values 99.0, 166.9, 281.2, 324.7. Bottom (from left to right): ionic intensity heatmaps of the ions at m/z values 428.7, 465.6, 518.6, 764.4.

Similarly, **P(VHar)** assisted laser ionization is also able to produce positive (Figure 7, m/z = 86.0, 104.0, 184.0, 554.5, 748.6, 798.4, 844.4, 874.4) as well as negative ions (Figure 8, m/z = 87.0, 89.0, 124.0; 145.0, 283.2, 346.0, 835.4, 887.5) directly on the tissue section. **P(VHar)** thus enables dual-mode measurements also in MALDI MS Imaging experiments. Enlarged pictures of the heatmaps are shown in the SI (Figures S153-S168).

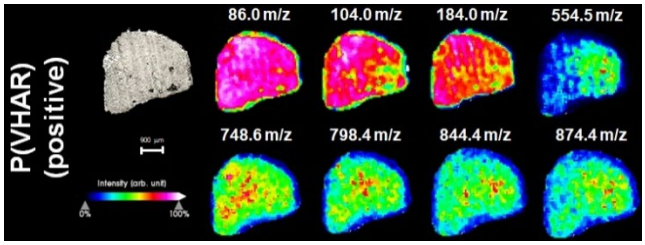

Figure 7. Positive mode MALDI MS Imaging measurements of a cryosection from a patient-derived breast cancer xenograft tumor

using **P(VHar)** as matrix. Top (from left to right) optical pictures, ionic intensity maps of ions at m/z values 86.0, 104.0, 184.0, 554.5. Bottom (from left to right) ionic intensity heatmaps of the ions at m/z values 748.6, 798.4, 844.4, 874.4.

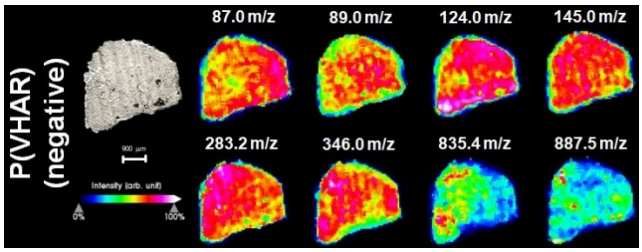

Figure 8. Negative mode MALDI MS Imaging measurements of a cryosection from a patient-derived breast cancer xenograft using **P(VHar)** as matrix. Top (from left to right) optical pictures, ionic intensity maps of ions at m/z values 87.0, 89.0, 124.0, 145.0. Bottom (from left to right) ionic intensity heatmaps of the ions at m/z values 283.2, 346.0, 835.4, 887.5.

These observations suggest that an ionization process assisted by **P(VDHB)** and **P(VHar)** occurs specifically on the tissue, showing that both P(SOMs) are well suitable as dual mode matrices for MALDI MS Imaging. The sample preparation via spray coating resulted in a smooth and homogeneous matrix coverage of the tissue section (Figure S136). Contrary to SOMs, the spraying process of the P(SOMs) required only very low concentrated matrix solutions (0.5 mg/ml), resulting in lower material consumption and less contamination of the sprayer machine. Additionally, in contrast to previously reported conjugated polymer matrices,[38] the P(SOMs) are well soluble in polar/protic solvents such as methanol, supporting analyte extraction from the tissue and leading to better signal intensities. Like for the corresponding SOMs, the solution composition influences the analyte extraction ability of the P(SOMs):[50] The production of ions in the range from 700 m/z - 960 m/z increases when the proportion of water is increased (Figure S134). Furthermore, the spatial localization of the exemplary ion at 846.4 m/z was improved by adding acetone in the matrix solution. Although SOMs often require additives, e.g. ammonium sulfate, to improve the detection limits for MALDI MS Imaging experiments, the used P(SOM) solutions, while being prepared without any additives, still led to sufficient signal intensities.[51-52] The MALDI silent properties of the P(SOMs), indicated by the single analyte measurement, are also observed during MALDI MS Imaging experiments: For example, a P(VDHB) heatmap of 155 m/z (protonated molecule ion of DHB) is completely black, hence shows no signal distribution, while a heatmap derived from using DHB is colorful (Figure S135). Consequently, P(VDHB) allows to measure and visualize isomers of DHB with a molar mass of 155 m/z. Also, the use of MALDI silent P(SOMs) prevents the detector from damage caused by strong matrix molecule bombardment when using higher laser intensities that is required to enhance the ionic intensities during MALDI MS Imaging experiments.[53]

CONCLUSION

Retaining the advantages of SOMs such as broad analyte scopes and high ionization efficiencies while also being MALDI silent and vacuum stable would allow to reliably and reproducibly measure LMWCs with MALDI MS and MS Imaging. Here, we present polymerization as a new strategy to achieve this. Two high performance SOMs (DHB and harmine) were modified to contain a vinyl group and polymerized to the corresponding polyethylene-based P(SOM), carrying SOMs as sidechains. The investigated P(VDHB) and P(VHar) are fully vacuum stable after 72h in UHV (~10^{-7} mbar), whereas either of the corresponding SOMs lost almost one third of their original masses within the same period. The P(SOMs) show very good absorption behavior, similar to the corresponding SOMs. Single analyte measurements of several commercially available lipids and saccharides indicate that both P(SOMs) have a similar analyte scope compared to their corresponding SOMs. P(SOMs) exhibited slightly higher ionization efficiencies, while also being MALDI silent. Also, the P(SOMs) were successfully used for MALDI MS Imaging experiments of breast cancer xenograft models, and allowed measurements in dual-mode without the utilization of additives. The obtained results are a promising foundation for future research efforts, e.g. for investigating the intra-patient and inter-patient reproducibility to enable new clinical MSI routines.

In summary, we present the polymerization of SOMs as a new strategy to obtain high performance MALDI matrix systems, which combine vacuum stability and MALDI silence with broad analyte scopes and high ionization efficiencies.

ASSOCIATED CONTENT

Supporting Information

A pdf file containing details about the used chemicals, the employed instrumentation, experimental settings and resulting data. The Supporting Information is available free of charge on the ACS Publications website.

AUTHOR INFORMATION

Corresponding Author

*lissel@ipfdd.de

Notes

The authors declare no competing financial interest.

ACKNOWLEDGMENT

The work was supported by KAUST Center Partnership Fund OSR-2017-CPF-3322-01. F.L. thanks the FCI for a Liebig Fellowship. Z.Q. thanks China Scholarship Council for a scholarship (no. 201908080098). The authors thank Christina Harnisch and Petra Treppe for providing GPC measurements and Dr. Mikhail Malanin for measuring FTIR-spectra. Mass spectrometry imaging experiments were supported by Norwegian Cancer Society, grant no. 198069. The authors thank the Cellular and Molecular Imaging Core Facility (CMIC) for the tissue sectioning.

REFERENCES

1. Croxatto, A.; Prod'hom, G.; Greub, G., *FEMS Microbiol. Rev.* **2012,** *36* (2), 380-407.
2. Norris, J. L.; Caprioli, R. M., *Chem. Rev.* **2013,** *113*, 2309-2342.
3. Vaysse, P.-M.; Heeren, R. M. A.; Porta, T.; Balluff, B., *Analyst* **2017,** *142*, 2690-2712.
4. Llombart, V.; Trejo, S. A.; Bronsoms, S.; Morancho, A.; Ma, F.; Faura, J.; Garcia-Berrocoso, T.; Simats, A.; Rosell, A.; Canals, F.; Hernandez-Guillamon, M.; Montaner, J., *J Proteomics* **2017,** *152*, 243-253.
5. Rauser, S.; Marquardt, C.; Balluff, B.; Deininger, S.-O.; Albers, C.; Belau, E.; Hartmer, R.; Suckau, D.; Specht, K.; Ebert, M. P.; Schmitt, M.; Aubele, M.; Höfler, H.; Walch, A., *J. Proteome Res.* **2010,** *9*, 1854-1863.

6. Liu, H.; Chen, R.; Wang, J.; Chen, S.; Xiong, C.; Wang, J.; Hou, J.; He, Q.; Zhang, N.; Nie, Z.; Mao, L., *Anal. Chem.* **2014,** *86*, 10114-10121.
7. Wang, J. S. H.; Freitas-Andrade, M.; Bechberger, J. F.; Naus, C. C.; Yeung, K. K. C.; N.Whitehead, S., *Rapid Commun. Mass Spectrom.* **2018,** *32*, 951–958.
8. Weigt, D.; Sammour, D. A.; Ulrich, T.; Munteanu, B.; Hopf, C., *Sci Rep* **2018,** *8*, 11260.
9. Giampa, M.; Lissel, M. B.; Patschkowski, T.; Fuchser, J.; Hans, V. H.; Gembruch, O.; Bednarza, H.; Niehaus, K., *Chem. Commun.* **2016,** *52*, 9801-9804.
10. Strupat, K.; Karas, M.; Hillenkamp, F., *Int. J. Mass Spectrom. Ion Processes* **1991,** *111*, 89-102.
11. Bourcier, S.; Bouchonnet, S.; Hoppilliard, Y., *Int. J. Mass Spectrom. Ion Processes* **2001,** *210/211*, 59-69.
12. Choi, S.-S.; Ha, S.-H., *Bull. Korean Chem. Soc.* **2007,** *28* (12), 2508-2510.
13. Lee, A.; Yang, H.-J.; Kim, Y.; Kim, J., *Bull. Korean Chem. Soc.* **2009,** *30* (5), 1127-1130.
14. Wei, Y.; Zhang, Y.; Lin, Y.; Li, L.; Liu, J.; Wang, Z.; Xiong, S.; Zhao, Z., *Analyst, 2015, 140, 1298* **2015,** *140*, 1298-1305.
15. Schiller, J.; Süß, R.; Fuchs, B.; Müller, M.; Petkovic, M.; Zschörnig, O.; Waschipky, H., *Eur. Biophys. J.* **2007,** *36*, 517–527.
16. Colsch, B.; Woods, A. S., *Glycobiology* **2010,** *20* (6), 661-667.
17. Perry, W. J.; Patterson, N. H.; Prentice, B. M.; Neumann, E. K.; Caprioli, R. M.; Spraggins, J. M., *J Mass Spectrom.* **2020,** *55*, 4491.
18. Dufresne, M.; Patterson, N. H.; Norris, J. L.; Caprioli, R. M., *Anal. Chem.* **2019,** *91*, 12928−12934.
19. He, H.; Qin, L.; Zhang, Y.; Han, M.; Li, J.; Liu, Y.; Qiu, K.; Dai, X.; Li, Y.; Zeng, M.; Guo, H.; Zhou, Y.; Wang, X., *Anal. Chem.* **2019,** *91*, 2634−2643.
20. Son, J.; Cha, S., *Bull. Korean Chem. Soc.* **2014,** *35* (5), 1409-1412.
21. Jun, C.; Tianxi, H.; Xuemei, F., *Talanta* **2012,** *100*, 419–424.
22. Lin, Y.-S.; Chen, Y.-C., *Anal. Chem.* **2002,** *74*, 5793-5798.
23. Tseng, M.-C.; Obena, R.; Lu, Y.-W.; Lin, P.-C.; Lin, P.-Y.; Yen, Y.-S.; Lin, J.-T.; Huang, L.-D.; Lu, K.-L.; Lai, L.-L.; Lin, C.-C.; Chen, Y.-J., *J. Am. Soc. Mass Spectrom.* **2010,** *21*, 1930–1939.
24. Mank, M.; Stahl, B.; Boehm, G., *Anal. Chem.* **2004,** *76*, 2938-2950.
25. Abdelhamida, H. N.; Gopala, J.; Wu, H.-F., *Anal. Chim. Acta* **2013,** *767*, 104–111.
26. Nonami, H.; Fukui, S.; Erra-Balsells, R., *J. Mass Spectrom.* **1997,** *32*, 287-296.
27. Cai, Y.; Jiang, Y.; Cole, R. B., *Anal. Chem.* **2003,** *75*, 1638-1644.
28. Yamagaki, T.; Suzuki, H.; Tachibana, K., *J. Am. Soc. Mass Spectrom.* **2007,** *18*, 714–723.
29. Nonami, H.; Tanaka, K.; Fukuyama, Y.; Erra-Balsells, R., *Rapid Commun. Mass Spectrom.* **1998,** *12*, 285–296.
30. Ropartz, D.; Bodet, P. E.; Przybylski, C.; Gonnet, F.; Daniel, R.; Fer, M.; Helbert, W.; Bertrand, D.; Rogniaux, H., *Rapid Commun. Mass Spectrom.* **2011,** *25*, 2059–2070.
31. Liu, H.; Zhou, Y.; Wang, J.; Xiong, C.; Xue, J.; Zhan, L.; Nie, Z., *Anal. Chem.* **2018,** *90*, 729−736.
32. Ling, L.; Xiao, C.; Ma, Y.; Jiang, L.; Wang, S.; Guo, L.; Jiang, S.; Guo, X., *Anal. Chem.* **2019,** *91*, 8801−8807.
33. Li, B.; Sun, R.; Gordon, A.; Ge, J.; Zhang, Y.; Li, P.; Yang, H., *Anal. Chem.* **2019,** *91*, 8221−8228.
34. Huang, P.; Huang, C.-Y.; Lin, T.-C.; Lin, L.-E.; Yang, E.; Lee, C.; Hsu, C.-C.; Chou, P.-T., *Anal. Chem.* **2020,** *92*, 7139−7145.
35. Arakawa, R.; Kawasaki, H., *Anal. Sci.* **2010,** *26*, 1229-1240.
36. Liang, Q.; Sherwood, J.; Macher, T.; Wilson, J. M.; Bao, Y.; Cassady, C. J., *J. Am. Soc. Mass Spectrom.* **2017,** *28*, 409-418.
37. Zhao, H.; Li, Y.; Wang, J.; Cheng, M.; Zhao, Z.; Zhang, H.; Wang, C.; Wang, J.; Qiao, Y.; Wang, J., *Appl. Mater. Interfaces* **2018,** *10*, 37732−37742.
38. Horatz, K.; Giampà, M.; Karpov, Y.; Sahre, K.; Bednarz, H.; Kiriy, A.; Voit, B.; Niehaus, K.; Hadjichristidis, N.; Michels, D. L.; Lissel, F., *J. Am. Chem. Soc.* **2018,** *140*, 11416−11423.
39. Horatz, K.; Ditte, K.; Prenveille, T.; Zhang, K.-N.; Jehnichen, D.; Kiriy, A.; Voit, B.; Lissel, F., *ChemPlusChem* **2019,** *84* (9), 1338-1345.
40. Bergamaschi, A.; Hjortland, G. O.; Triulzi, T.; Sørlie, T.; Johnsen, H.; Ree, A. H.; Russnes, H. G. i.; Tronnes, S.; Mælandsmo, G. M.; Fodstad, O.; Borresen-Dale, A.-L.; Engebraaten, O., *Mol. Oncol.* **2009,** *3* (5-6), 469-482.
41. Su, W.-F., Radical Chain Polymerization. In *Principles of Polymer Design and Synthesis. Lecture Notes in Chemistry*, Springer, Berlin, Heidelberg: 2013; Vol. 82, pp 137-183.
42. Ponce, M. A.; Erra-Balsells, R., *J. Heterocyclic Chem.* **2001,** *38*, 1087.
43. McNaught, A. D.; Wilkinson, A., *IUPAC. Compendium of Chemical Terminology*. 2 ed.; Blackwell Scientific Publications: 1997.
44. Astigarraga, E.; Barreda-Gomez, G.; Lombardero, L.; Fresnedo, O.; Castano, F.; Giralt, M. T.; Ochoa, B.; Rodriguez-Puertas, R.; Fernandez, J. A., *Anal. Chem* **2008,** *80*, 9105–9114.
45. Glunde, K.; Jie, C.; Bhujwalla, Z. M., *Cancer Res.* **2004,** *64*, 4270–4276.
46. Shariatgorji, M.; Nilsson, A.; Goodwin, R. J. A.; Källback, P.; Schintu, N.; Zhang, X.; Crossman, A. R.; Bezard, E.; Svenningsson, P.; Andren, P. E., *Neuron* **2014,** *84*, 697–707.
47. Natrajan, R.; Sailem, H.; Mardakheh, F. K.; Garcia, M. A.; Tape, C. J.; Dowsett, M.; Bakal, C.; Yuan, Y., *PLOS Medicine* **2016,** *13*, e1001961.
48. Hasebe, T., *Expert Opinion on Therapeutic Targets* **2013,** *17* (4), 449-460.
49. Balluff, B.; Frese, C. K.; Maier, S. K.; Schöne, C.; Kuster, B.; Schmitt, M.; Aubele, M.; Höfler, H.; Deelder, A. M.; Heck, A. J.; Hogendoorn, P. C.; Morreau, J.; Altelaar, A. M.; Walch, A.; McDonnell, L. A., *J. Pathol.* **2015,** *235*, 3-13.
50. Bashirc, S.; Mutter, R.; Derrick, P. J., *Eur. J. Mass Spectrom.* **2004,** *10* (4), 487-493.
51. AlMasoud, N.; Correa, E.; Trivedi, D. K.; Goodacre, R., *Anal.Chem.* **2016,** *88*, 6301-6308.
52. Sugiyama, E.; Masaki, N.; Matsushita, S.; Setou, M., *Anal. Chem* **2015,** *87*, 11176−11181.
53. Guenther, S.; Koestler, M.; Schulz, O.; Spengler, B., *Int. J. Mass Spectrom. Ion Processes* **2010,** *294*, 7-15.

TOC-graphic

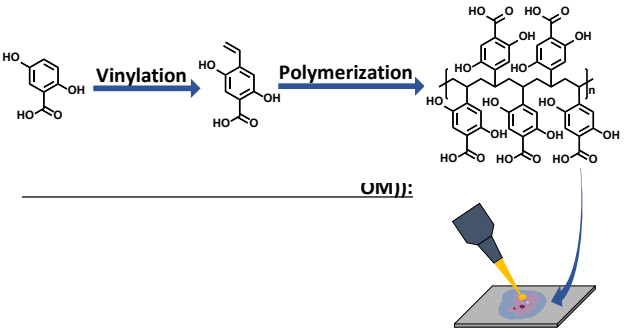

OM)):